Dense Motion Estimation from Eye-Safe Aerosol Lidar Data

Pierre Dérian, Patrick Héas, Etienne Mémin, Shane Mayor

DENSE MOTION ESTIMATION FROM EYE-SAFE AEROSOL LIDAR DATA

Pierre Dérian[1], Patrick Héas[1], Étienne Mémin[1], Shane D. Mayor[2]

[1]*INRIA Rennes - Bretagne Atlantique, 35042 Rennes Cedex, FRANCE. Email: Pierre.Derian@inria.fr, Patrick.Heas@inria.fr, Etienne.Memin@inria.fr*

[2]*Department of Physics, California State University Chico, Chico, California, 95929, USA. E-mail: sdmayor@csuchico.edu*

ABSTRACT

Results of the application of optical flow methods to eye-safe aerosol lidar images leading to dense velocity field estimations are presented. A fluid motion dedicated formulation is employed, taking into account the deforming shapes and changing brightness of flow visualization. The optical flow technique has the advantage of providing a vector at every pixel in the image, hence enabling access to improved multiscale properties. In order to assess the performances of the method, we compare vectors with punctual sonic anemometer measurements. Power spectra of the velocity data are also calculated to explore the spectral behavior of the technique.

1. INTRODUCTION

The determination of air motion vectors from images produced by scanning aerosol lidars has previously been accomplished by computing cross-correlation functions from two or more frames in time [1]. For a spatially resolved vector flow field, the correlation functions can be computed for sub-regions of the full images [2]. Although being fast and robust, those methods produce sparse vector fields and it is a challenge to obtain information near the edges of the scan area. In this new work, we apply an optical flow algorithm to calculate dense motion vectors from scanning eye-safe aerosol lidar images. Optical flow technics have been proposed in the computer vision domain in order to infer scene motion measurements. Dense motion vectors are routinely computed for machine vision, digital video compression, and camera surveillance. Recently, optical flow has also been applied to images of fluid motion [3, 4, 5]. This is a more challenging problem than the case of tracking solid objects because the features related to the flow visualization typically have deforming shapes and changing brightness. In order to tackle this difficulty, appropriate smoothing functions on the velocity field and sound variation models linking the velocity unknown to the image luminance variation have to be proposed. This paper is a companion to the one by S. D. Mayor [6] in the same conference. Details about the lidar, the experiment, and the vectors computed via the correlation method can be found in that paper.

2. OPTICAL FLOW METHODS

2.1. Standard formulation

Optical-flow estimation aims at recovering the apparent displacement field $\mathbf{w} = (u, v)^T$ between two consecutive frames in an image sequence. This classical computer-vision problem is solved through the minimization of some energy function $J = J_{obs} + J_{reg}$, initially formulated by Horn & Schunck [7]. The first term J_{obs} constitutes a data model that links the displacement field to be estimated to information from image pairs through the *optical-flow constraint* (OFC). This constraint states that luminance $f(s,t)$ at a given point $s \in \Omega$ remains constant along its trajectory: $\frac{df(s,t)}{dt} = 0$. The data model enforces this behavior through the following cost function:

$$J_{obs}(\mathbf{w}) = \int_\Omega \phi\left(\nabla f(s).\mathbf{w}(s) + \frac{\partial f(s)}{\partial t}\right) ds \qquad (1)$$

where ϕ might be the L_2 norm or some robust function to deal with strong deviation from the OFC data-model. The second term J_{reg} is a regularization term, classically a first order penalization is used:

$$J_{reg}(\mathbf{w}) = \alpha \int_\Omega \phi\left(\|\nabla \mathbf{w}\|\right) ds \qquad (2)$$

Here parameter α controls the balance of the OFC data-model and the smoothness of the estimated field $\mathbf{w}$.

2.2. Fluid motion estimation

The two terms of the energy function J have been modified in order to take into account physical properties of the fluid motion. The OFC constraint (1) has been replaced by the *integrated continuity equation* (ICE), based on mass conservation [8]:

$$J_{obs}(\mathbf{w}) = \int_\Omega \phi\left(\frac{\partial f(s)}{\partial t} + div(f(s)\mathbf{w})\right) ds \qquad (3)$$

The first-order regularization (2) penalizes the gradient of the estimated field $\mathbf{w}$ and enforces low divergence and vorticity. A second order regularization has been proposed [3] which instead penalizes gradients and favors blobs of both vorticity and divergence :

$$J_{reg}(\mathbf{w}) = \alpha \int_\Omega \phi\left(\|\nabla curl\mathbf{w}\| + \|\nabla div\mathbf{w}\|\right) ds \qquad (4)$$

where $curl\mathbf{w} = \frac{\partial v}{\partial x} - \frac{\partial u}{\partial y}$ and $div\mathbf{w} = \frac{\partial u}{\partial x} + \frac{\partial v}{\partial y}$ respectively denote vorticity and divergence of $\mathbf{w}$. Those modifications have proven to be efficient for fluid motion estimation in various cases such as particle image velocimetry (PIV) or satellite imagery [3, 4].

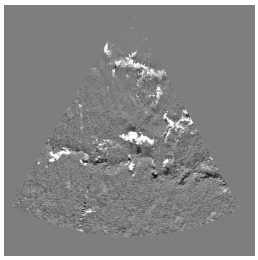

Figure 1: Example of input image data for dense motion estimation .

3. APPLICATION TO LIDAR IMAGES

3.1. Experiment

Data was collected by a $1.5\,\mu\mathrm{m}$ eye-safe aerosol lidar as a part of the 2007 CHATS measurement campaign, which also includes in-situ measurements recorded at a $60\,\mathrm{Hz}$ sample rate from a micro-meteorological tower located within the lidar scan plane. More information on the lidar, this experiment and its results can be found in papers by S.D. Mayor [9, 10]. Preprocessing of raw data – such as interpolation from polar to cartesian coordinates – leads to $602 \times 602\,\mathrm{px}$ frames of $10\,\mathrm{m}$ resolution. Each frame has an associated mask describing the cone-shaped data area – see fig. 1. This mask enables the discarding of irrelevant pixels for the estimation process.

Optical flow methods have been applied to two different lidar data cases. These two cases were chosen because of their sharply contrasting differences in flow dynamics. The case from April 26 took place in a turbulent convective boundary layer and included the passage of a density current front; the case from March 21 occurs in a weakly stable evening boundary layer with light winds. In this case, stability suppresses turbulence and supports the existence of "gravity" waves. In the March 21 case the wind speeds are low and the wind direction is constantly changing. In the April 26 case, the wind speeds are stronger and the direction is more consistent except for near reversal with the passage of the front.
The March 21 case consists of 536 frames ranging between 04:15 and 6:59 with a time-step of $17.3\,\mathrm{s}$, while the April one shows 358 frames from 22:00 to 01:00 on 27 April 2007 with a $30\,\mathrm{s}$-interval between two consecutive frames. Both cases have been investigated using the same set of parameters:

- ICE data model;
- Div-Curl regularization;
- robust behavior to discard irrelevant pixels;
- no temporal coherence: frames are treated as independent consecutive pairs.

The estimated velocity fields have the same resolution as the input frames, i.e. $602 \times 602\,\mathrm{px}$. Figure 2 shows an example of the estimated vectors with associated vorticity and divergence map. The in-situ measurement tower is located $1600\,\mathrm{m}$ south of the lidar site, and does sometimes appear on the input frame as few bright pixels of maximum size $2 \times 2\,\mathrm{px}$. Thanks to the use of the robust data term, those pixels are sometimes discarded by the algorithm. In order to compare tower measurements with reliable estimated values, the latter are averaged over a $4 \times 4\,\mathrm{px}$ box centered on the tower location. Tower measurements, originally sampled at $60\,\mathrm{Hz}$, are also averaged over $15\,\mathrm{s}$-windows centered on the times of the frames.

3.2. Wind Speed and Direction

Figure 3 shows a comparison of wind speed and its direction between averaged anemometer data and estimated ones. The first case – March 21 – shows a good agreement between estimation and measurements for both norm and direction, except for two short periods where the direction strongly deviated. The second case, April 26, is much more turbulent, with a higher amount of scatter in both anemometer and estimated wind speed. However, being much more stable, wind direction is well retrieved.

3.3. Spectra

Figure 4 represents time-power spectral densities (PSD) computed using a Welch estimator. Lidar frame rate is much lower than the anemometer sample rate, hence its spectra are only defined over low frequencies. Observations from wind speed comparisons are confirmed: PSDs are in reasonable agreement for the 21 March case, up to the lidar Nyquist frequency where a "pile-up" of energy appears, not present in the anemometer data. Some energy is also missing at the estimated middle scales ($\sim 10^{-3}\,\mathrm{Hz}$), it might have been caused by a too strong regularization. For the April 26 "turbulent case", it appears that the algorithm under-estimates the PSD over a broad range of scales, not surprisingly since wind speed was badly retrieved. Both cases show an inertial cascade with a $-\frac{5}{3}$ slope, unfortunately occurring at temporal scales unreachable through lidar frames. Figure 5 shows time-averaged spatial spectra computed from a $256 \times 256\,\mathrm{px}$ box extracted from the estimated velocity fields. A power-law fit gives a slope of ~ -2.

4. CONCLUSION

Optical flow methods with fluid-motion dedicated formulation have been applied to lidar data frames. Results are in good agreement with in-situ measurements, although particular dynamics might mislead the algorithm. The development of a lidar-dedicated data model combined with the utilization of turbulence dynamics multiscale regularization [5] should lead to improved dense motion estimations.

ACKNOWLEDGMENTS

S. D. Mayor's participation in this collaboration was made possible by NSF AGS award 0924407.

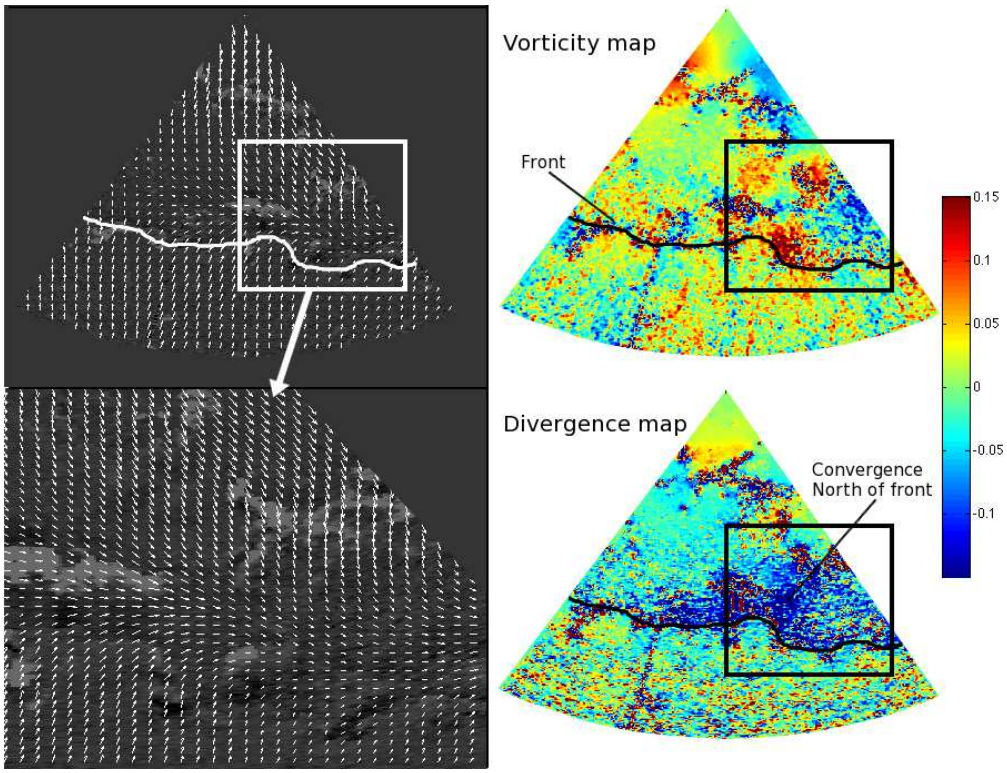

Figure 2: Example of estimated dense field – 26 April, 23:05:41. The close-up (bottom-left) shows two counter-rotating vortices situated near the northward moving density front; velocity vectors are superimposed every 6 px on the input frame. Up-right is vorticity map confirming the two vortices, bottom-right is the divergence map showing convergence north of the front.

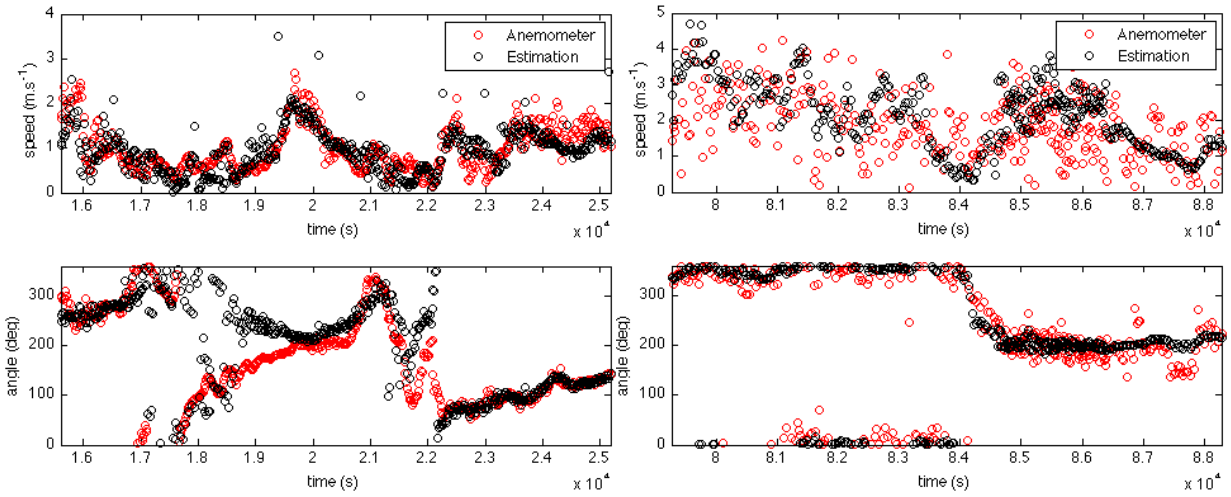

(a) 21 March 2007

(b) 26 April 2007

Figure 3: Comparison of wind speed (top) and direction (bottom) between anemometer data (red circles) and estimated velocities with optical flow method (black circles) for 21 March (left column) and 26 April (right column).

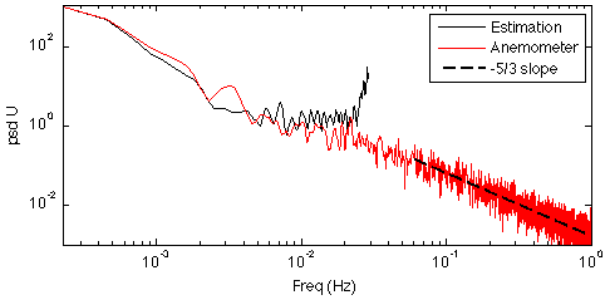

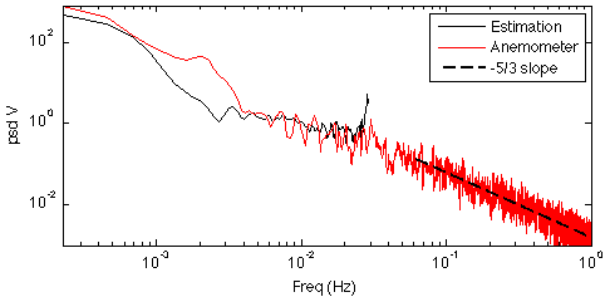

(a) 21 March 2007

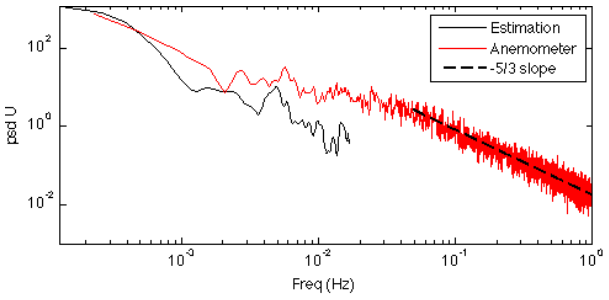

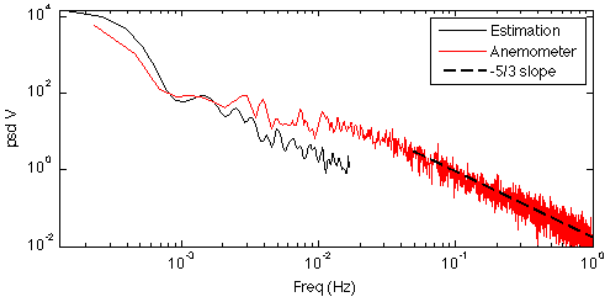

(b) 26 April 2007

Figure 4: Comparison of time PSDs computed for the 2 data set from anemometer data (red) and estimated field (black) for U (top) and V (bottom)

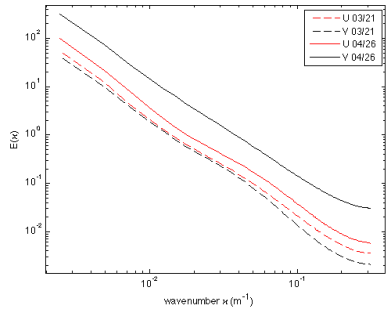

Figure 5: Time-averaged spatial PSD computed from estimated field (black) for U (top) and V (bottom)

REFERENCES

1. Schols, J. and Eloranta, E. 1992: Calculation of area-averaged vertical profiles of the horizontal wind velocity from volume-imaging lidar data. *Journal of geophysical research*, 97(D 17):18395–18407.

2. Mayor, S. and Eloranta, E. 2001: Two-dimensional vector wind fields from volume imaging lidar data. *Journal of Applied Meteorology*, 40:1331–1346.

3. Corpetti, T., Heitz, D., Arroyo, G., Mémin, E., and Santa-Cruz, A. 2006: Fluid experimental flow estimation based on an optical-flow scheme. *Experiments in Fluids*, 40:80–97.

4. Héas, P., Mémin, E., Papadakis, N., and Szantai, A. 2007: Layered estimation of atmospheric mesoscale dynamics from satellite imagery. *IEEE Transactions on Geoscience and Remote Sensing*, 45:4087–4104.

5. Héas, P., Mémin, E., Heitz, D., and Mininni, P. 2009: Bayesian selection of scaling laws for motion modeling in images. In *Int. Conf. on Computer Vision*.

6. Mayor, S. 2010: Horizontal Motion Vectors From Cross-correlation: First Application To Eye-safe Aerosol Lidar Data From Chats. In *25th Int. Laser Radar Conf.*.

7. Horn, B. and Schunck, B. 1981: Determining Optical Flow. *Artificial Intelligence*, 17:185–203.

8. Corpetti, T., Mémin, É., and Pérez, P. 2002: Dense estimation of fluid flows. *IEEE Transactions on pattern analysis and machine intelligence*, pp. 365–380.

9. Mayor, S. 2008: Observations of Sea-breeze Fronts and Turbulence Near the Surface During Stable Conditions. In *24th Int. Laser Radar Conf.*, pp. SO30–01.

10. Mayor, S., Spuler, S., Morley, B., and Loew, E. 2007: Polarization lidar at 1.54 μm and observations of plumes from aerosol generators. *Optical Engineering*, 46:096201.